(Received 5 August 2025, Accepted 1 October 2025, Scheduled 10 October 2025)

# Doublet-Based Tunable Bandstop Filters with Wide Frequency Tuning Range and Constant Bandwidth

Qi Zheng[1,2], Pengyu Yu[3], Yuhua Cheng[1,2], and Pengde Wu[1,2,*]

[1] *The Key Laboratory of Micro-Nano Sensing and IoT of Wenzhou Wenzhou Institute of Hangzhou Dianzi University, Wenzhou 325038, China*
[2] *The School of Electronics and Information, Hangzhou Dianzi University, Hangzhou 311101, China*
[3] *The Department of Electronic Engineering, the Chinese University of Hong Kong, Hong Kong, China*

**ABSTRACT:** This paper introduces a novel method for designing a wideband tunable bandstop filter (BSF) with constant absolute bandwidth (ABW). The design uses a doublet configuration, where two varactor-tuned resonators are symmetrically coupled to a main transmission line. To maintain constant ABW during frequency tuning, a coupling scheme is proposed where coupling strength decreases as the frequency increases, eliminating the need for additional circuits. Theoretical analysis and closed-form equations are provided for designing the BSF with a wide tuning range. A BSF prototype is designed and tested, demonstrating a 10-dB ABW of approximately 190 MHz across a continuous stopband tuning range from 3.3 to 5.1 GHz, with a fractional tuning range of 42.9%.

## 1. INTRODUCTION

Bandstop filters (BSFs) have become essential in wireless communication systems due to their ability to suppress unwanted bands, including harmonics, spurious signals, and out-of-band noise [1, 2]. In practical applications, BSFs with constant absolute bandwidth (ABW) are highly attractive for practical applications requiring adaptive interference suppression, particularly in 5G systems, where coexistence with legacy networks and adjacent-band services poses significant challenges [3, 4]. For instance, in sub-6 GHz 5G deployments (e.g., n77/n78), tunable BSFs can mitigate strong interference from neighboring C-band satellite downlinks or Wi-Fi systems, thereby improving receiver sensitivity and spectral efficiency [5, 6]. Beyond 5G, they also play an essential role in cognitive radios, software-defined radios, satellite communications, and radar systems by dynamically nulling unwanted signals in congested or contested spectral environments [7].

In recent years, various techniques have been developed to improve the adaptability of tunable BSFs. Among them are four well-known tuning methods. First, magnetic materials [8, 9] such as yttrium-iron-garnet (YIG) enable frequency tuning but consume considerable direct current (DC) power. Second, tunable BSFs based on varactor-tuned resonators or defected ground structure (DGS) configurations [10, 11] have more compact designs compared to the magnetic materials, but they may struggle with bandwidth stability during tuning. Third, micro-electromechanical system (MEMS) technology, which provides miniaturization and high quality factors [12, 13], is attracting increasing interest in tunable BSF designs [14, 15]. Nevertheless, MEMS may face reliability issues in harsh environments. Lastly, ferroelectric components are increasingly utilized in tunable filter designs due to their ability to dynamically adjust dielectric constants based on applied electric fields [16, 17]. While this technique offers more design parameters for tuning, it is more sensitive to temperature variations.

To maintain a constant ABW independent of tuned center frequency, the inter-resonator coupling needs to be controlled to vary inversely with the tuning frequency. In [18], a design achieved constant ABW without additional control circuits by allowing electric and magnetic coupling strengths within a fixed coupling region to vary oppositely with frequency. In [19], a matematerial-based BSF used an electromagnetic bandgap structure embedded within a microstrip line, but it required a perforated dielectric plate directly placed on the surface of the microstrip line to maintain constant ABW, complicating tuning.

This paper presents a simple approach to designing frequency-tuning BSFs with a constant ABW. The proposed coupling scheme adjusts the coupling strength in opposite directions as the frequency changes, allowing the coupling strength to naturally decrease with the increase of the stopband frequency, thereby achieving a constant ABW without the need for additional control circuits. Closed-form equations for the tunable BSF are provided, along with theoretical predictions and experimental results.

## 2. ANALYSIS OF THE DOUBLET

### 2.1. Tunability of the Resonator

Figure 1 shows the proposed tunable BSF with a doublet configuration. It consists of two coupled-line sections and a through transmission line in the middle. The resonator is formed by the upper part of coupled lines, with one end open and the other

* Corresponding author: Pengde Wu (wupengde@hdu.edu.cn).

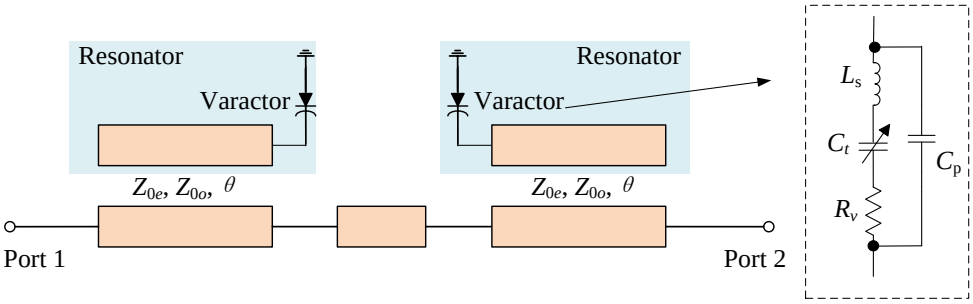


**FIGURE 1**. The proposed tunable bandstop filter with constant ABW based on doublet configuration. Varactor diode $C_t$ is employed to tune the resonant frequency of the resonator.

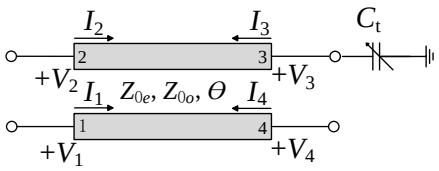


**FIGURE 2**. Definitions of port voltage and current for the varactor-tuned resonators.

terminated with a varactor. The varactor has an equivalent capacitance of $C_t$, and tuning the capacitance of $C_t$ changes the resonator's electrical length, allowing the stopband frequency to be adjusted. The equivalent circuit model of the varactor is shown in the right part of Fig. 1.

A zoomed-view of the proposed resonator is shown in Fig. 2 with definitions of port voltage and current. Considering the superposition of even- and odd-mode excitations, $ABCD$ matrix can be derived [20]. In the even-mode excitation, we have

$$\begin{bmatrix} \frac{1}{2}(V_1+V_2) \\ \frac{1}{2}(I_1+I_2) \end{bmatrix} = \begin{bmatrix} \cos\theta & j\,Z_{0e}\sin\theta \\ j\,Y_{0e}\sin\theta & \cos\theta \end{bmatrix} \cdot \begin{bmatrix} \frac{1}{2}(V_4+V_3) \\ -\frac{1}{2}(I_4+I_3) \end{bmatrix} \tag{1}$$

where $Z_{0e}$ and $Y_{0e}$ are the even-mode impedance and admittance, respectively. In the odd-mode excitation, we can show that

$$\begin{bmatrix} \frac{1}{2}(V_1-V_2) \\ \frac{1}{2}(I_1-I_2) \end{bmatrix} = \begin{bmatrix} \cos\theta & j\,Z_{0o}\sin\theta \\ j\,Y_{0o}\sin\theta & \cos\theta \end{bmatrix} \cdot \begin{bmatrix} \frac{1}{2}(V_4-V_3) \\ -\frac{1}{2}(I_4-I_3) \end{bmatrix} \tag{2}$$

where $Z_{0o}$ and $Y_{0o}$ are the odd-mode impedance and admittance, respectively.

As shown in Fig. 2, once port 2 is open-circuited and port 3 terminated with a capacitance of $C_t$, the boundary conditions for the four ports can be expressed as

$$I_2 = 0;\; V_3 = -\,I_3 \cdot Z_c \tag{3}$$

where $Z_c$ is the impedance of $C_t$.

Substituting (3) into (1) and (2) gives a two-port $ABCD$ matrix equation for ports 1 and 4, which is

$$\begin{bmatrix} V_1 \\ I_1 \end{bmatrix} = \begin{bmatrix} \frac{2a\cos\theta + Z_1 Y_1 \omega C_t \sin\theta}{2a} & j\frac{Z_2\sin\theta}{2} \\ j\frac{(aY_2 - Y_1^2)\sin\theta}{2a} & \cos\theta \end{bmatrix} \cdot \begin{bmatrix} V_4 \\ -I_4 \end{bmatrix}. \tag{4}$$

where $a = Y_2 + 2\omega\, C_t \cot\theta$, and

$$\begin{cases} Z_1 = Z_{0e} - Z_{0o};\; Z_2 = Z_{0e} + Z_{0o} \\ Y_1 = Y_{0e} - Y_{0o};\; Y_2 = Y_{0e} + Y_{0o} \end{cases}$$

According to the conversions between $ABCD$ and $S$-parameters, the transmission coefficient from port 1 to port 4 can be obtained as

$$S_{41} = \frac{4aZ_0}{Z_0\left(Z_1Y_1\omega C_t\sin\theta + 4a\cos\theta\right) + j\left(aZ_2 + aZ_0Y_2 - Z_0Y_1^2\right)\sin\theta} \tag{5}$$

where $Z_0$ is a load impedance. The transmission zero occurs when $S_{41} = 0$, which implies that

$$\omega\cot\theta = -\frac{Y_{0e}+Y_{0o}}{2\,C_t}. \tag{6}$$

Now if $\theta = \pi/2$ at frequency $f_0$, the relation between an arbitrary transmission zero $f$ and $C_t$ can be expressed as

$$\frac{f}{f_0}\cot\frac{\pi}{2}\frac{f}{f_0} = -\frac{Y_{0e}+Y_{0o}}{4\pi f_0 C_t}. \tag{7}$$

To have a better understanding of (7), its left and right terms are plotted in Fig. 3, and the intersection points of the two curves are the lower and upper bounds ($f_H/f_L$) of the frequency tuning range.

## 2.2. Bandwidth Control

To achieve the desired coupling strength that decreases with increasing frequency, we proposed a fixed coupling region where the coupling strength varies oppositely as the frequency

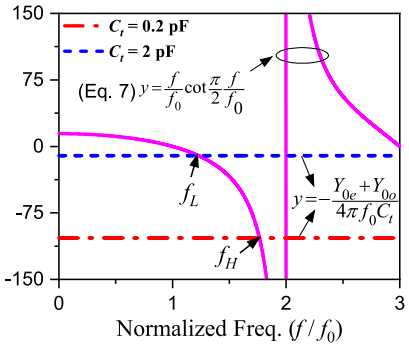


**FIGURE 3**. Solving Eq. (7) using the graphical method. Both left and right terms of Eq. (7) are plotted when $Y_{0e} = 0.015$, $Y_{0o} = 0.026$. The frequency is normalized to $f_0$ where $\theta = \pi/2$ at $f_0$.

changes. This mechanism allows for coupling coefficient control across different frequencies without additional circuits.

Figure 4 shows the equivalent circuit for the coupled-line section shown in Fig. 2. It is denoted by a transmission line in parallel with an admittance inverter $J$ [21]. The resonator is equivalent to the parallel connected inductor $L$ and capacitor $C_t$, and its resonant angular frequency is $w_r = 1/\sqrt{LC_t}$.

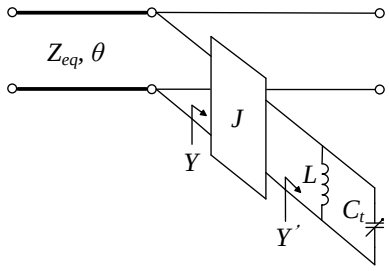


**FIGURE 4**. Equivalent circuit model for the coupled line section shown in Fig. 2.

The impedance of the resonator after it is transformed by the $J$-inverter is

$$Z_r = \frac{j\omega C_t + \frac{1}{j\omega L}}{J^2} \tag{8}$$

Using reactance slope parameter [18], the bandwidth can be expressed as

$$\Delta\omega = \frac{\omega_r}{2}\frac{Z_0}{\frac{\omega_r}{2}\frac{\partial \mathrm{Im}(Z_r)}{\partial\omega}\Big|_{\omega=\omega_r}} = \frac{Z_0 J^2}{2C_t}. \tag{9}$$

where $Z_0$ is the system impedance (usually 50 Ω).

Equation (9) indicates that the bandwidth $\Delta\omega$ is proportional to $J^2$ and inversely proportional to $C_t$. Since the resonant frequency decreases as $C_t$ increases, maintaining a constant ABW $\Delta\omega$ requires $J$ to decrease as the frequency increases. Furthermore, since $J$ is proportional to the coupling strength $C$ between the resonator and main line [21], to maintain a constant ABW, the coupling strength should decrease when the stopband frequency is tuned upward.

### 2.3. Bandwidth Control Scheme

The theoretical analysis for the relationship between the coupling strength and frequency can be found in [22]. For the ports defined in Fig. 2, in the case of weak coupling, we have

$$\frac{V_2}{V_1} \approx \frac{jk\tan\theta}{1+j\tan\theta} = jk\sin\theta e^{-j\theta} \tag{10}$$

where $k = (Z_{0e} - Z_{0o})/(Z_{0e} + Z_{0o})$. Once $\theta = \pi/2$ where the coupling section is $\lambda/4$ long, the coupling strength $C$ is expressed as

$$C = \left|\frac{V_2}{V_1}\right| = k\sin\frac{\pi}{2}\frac{f}{f_0}. \tag{11}$$

From Eq. (11), Fig. 5 plots the square of the coupling strength versus frequency when $k = 0.25$. It is observed that the square of the coupling strength decreases as the frequency increases from $f_0$ to $2f_0$. This behaviour ensures a constant ABW as long as the frequency tuning range $(f_L, f_H)$ remains within $f_0$ to $2f_0$.

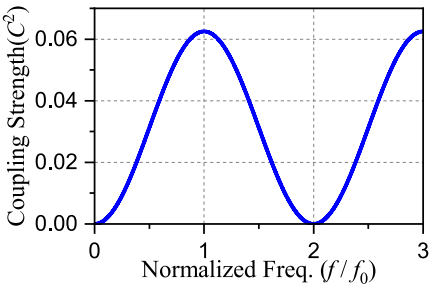


**FIGURE 5**. Coupling strength (squared) versus frequencies, which is normalized by $f_0$.

The even- and odd-mode characteristic impedances are as follows [22] when the coupling coefficient $k$ is determined

$$Z_{0e} = Z_0\sqrt{\frac{1+k}{1-k}}, \quad Z_{0o} = Z_0\sqrt{\frac{1-k}{1+k}}. \tag{12}$$

where $Z_0$ is usually 50 Ω.

In summary, the stopband frequency $f$ is set between $f_0$ and $2f_0$, with the coupling coefficient $k$ remaining constant once the coupled line section is fixed. Since the sine function in (11) monotonically decreases from $\pi/2$ to $\pi$, the coupling strength $C$ naturally decreases as the tuning frequency increases from $f_0$ to $2f_0$. Thus, the requirement of constant ABW can be satisfied. Based on the above analysis, the design procedures of the proposed tunable BSF with a constant ABW are summarized in Fig. 6. As shown, the design of the proposed tunable BSF with a constant ABW involves four key steps, which are:

1. Specify the frequency tuning range $(f_L, f_H)$ of interest and make sure $f_H/f_L < 1.6$ (theoretical maximum $f_H/f_L = 2$ ).

2. Select a reference frequency $f_0$ ensuring $f_0 < f_L$ and $f_H < 2f_0$, then the length of the coupled line is determined.

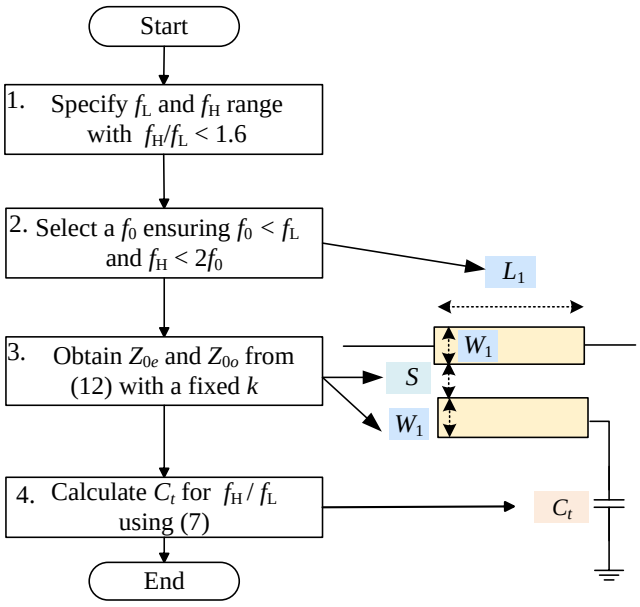


**FIGURE 6**. A flow chart for designing the proposed BSF with a constant ABW.

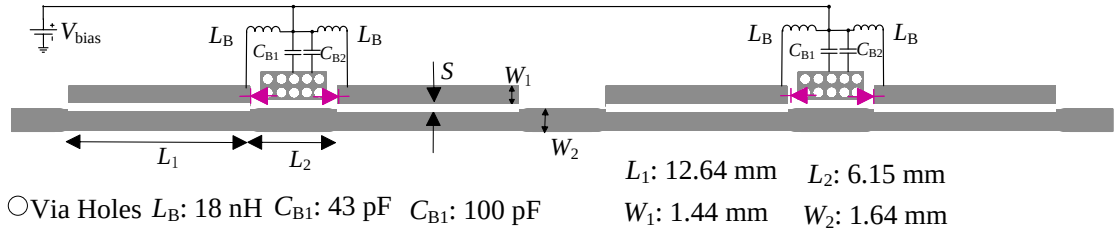


**FIGURE 7**. Layout of the proposed tunable BSF using varactor-based doublets configuration.

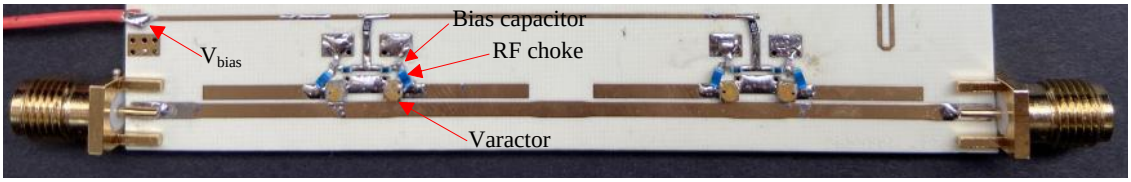


**FIGURE 8**. Fabricated tunable BSF with constant absolute bandwidth.

3. Calculate $Z_{0e}$ $Z_{0d}$ of the coupled line using Eq. (12) with a weak coupling coefficient $k$, then the width and gap of the coupled line are determined.

4. Calculate required $C_t$ for $f_H$ or $f_L$ using Eq. (7).

## 3. IMPLEMENTATION AND MEASUREMENT

Based on the previous analysis, the proposed tunable BSF with constant ABW was designed using four resonators. It was fabricated and implemented according to the physical dimensions indicated in Fig. 7. RO4350B ($\epsilon_r = 3.66$ and $\tan\delta = 0.0037$) with a thickness of 0.762 mm was used as the substrate. A photograph of the fabricated BSF is shown in Fig. 8, and the varactor is MA46H201 from MACOM, which is used as $C_t$. In this design, a coupling coefficient $k = 0.25$ is chosen for the fabrication constraint of the printed circuit board (PCB) process. Besides, $f_0$ was selected as 3.6 GHz, so the electrical length $\theta$ of the coupled-line is $\pi/2$ at $f_0$.

The simulation is accomplished by using full-wave simulator of advanced design system (ADS), and the varactor diode is represented by a full equivalent circuit which consists of a tunable capacitor $C_t$, a diode resistance $R_v$, packaging inductance $L_s$, and capacitance $C_p$ (see Fig. 1). According to the relationship between MA46H201's total capacitance and its reverse bias voltage, $C_t$ is chosen to vary from 0.4 to 2.4 pF in the simulation. Fig. 9 shows the simulated responses when tuning capacitance has six discrete values. As indicated in Fig. 9, the constant 10-dB ABW is around 200 MHz, and it remains nearly unchanged as the stopband center frequency increases from 3.48 to 5.21 GHz.

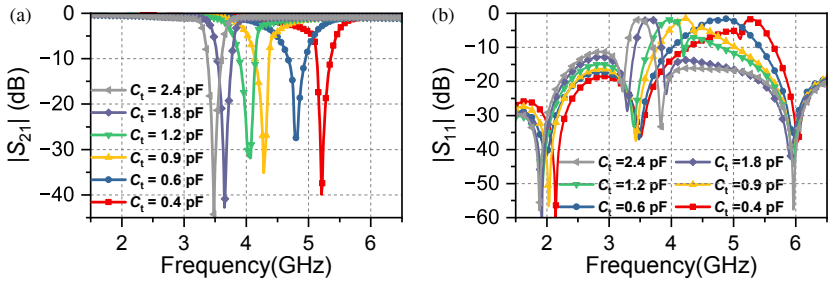


**FIGURE 9**. Simulated results of the proposed tunable BSF with different tuning capacitances. (a) $|S_{21}|$. (b) $|S_{11}|$.

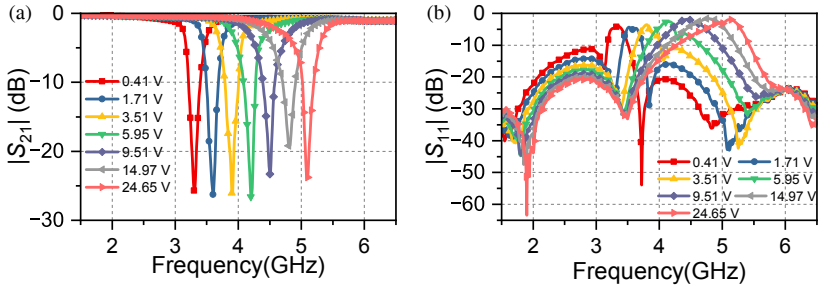


**FIGURE 10**. Measured frequency responses of the proposed tunable BSF under different biasing voltages. (a) $|S_{21}|$. (b) $|S_{11}|$.

**TABLE 1**. Comparisons with other published tunable BSFs.

| Ref. | Tuning range/GHz (%) | Constant ABW (MHz) | Tech. | Size (mm) |
|---|---|---|---|---|
| [6] | 3.22–3.66 (12.8% ) | 30 ± 1 (10-dB) | Dual-band combining | 110 × 40 |
| [18] | 1.73–2.2 (23.9%) | 60 ± 3 (40-dB) | Coupling scheme | 60 × 30 |
| [19] | 3.56–4.03 (12.3% ) | 244 ± 3.2 (10-dB) | Mechanical plate | 99.2 × 5.6 |
| [23] | 3.0–6 (46% ) | 46 ± 1.5 (10-dB) | Asynchronous tuning | 30 × 30 |
| This work | 3.3–5.1 (42.9%) | 190 ± 20 (10-dB) | Coupling scheme | 69 × 4 |

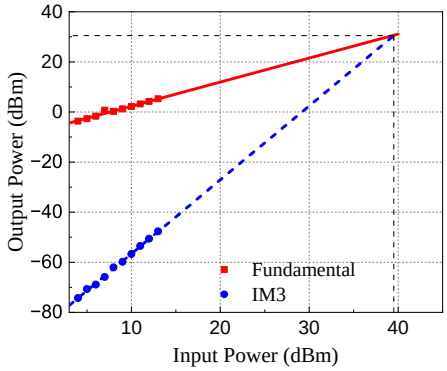


**FIGURE 11**. Measured output power of the fundamental signals and the IM3 against the input power at a bias voltage of 0.41 V.

The measured frequency responses are shown in Fig. 10. The stopband center frequency can be continuously tuned from 3.3 to 5.1 GHz, featuring a fractional tuning range of 42.9%. The attenuation levels at the mid-stopband exceed 20 dB, and the passband insertion loss is under 1.2 dB. The measured 10-dB ABW across various stopband frequencies is approximately 190 MHz with a maximum variation of 20 MHz, which can be considered constant.

According to the datasheet of varactor MA46H201, its capacitance is around 2.4 pF at a bias voltage of 0.4 V. Compared to the simulated $|S_{21}|$ with 2.4 pF, the measured $|S_{21}|$ at 0.4 V shows a frequency shift about 200 MHz, caused by the package inductance and capacitance of MA46H201. Additionally, the measured mid-stopband attenuation is lower than the simulation results due to the varactor's junction resistance.

The input third-order intercept point (IIP3) of the proposed BSF was measured by a spectrum analyzer and two signal generators with two closely spaced frequencies of 3.000 and 3.002 GHz. As can be seen in Fig. 11, when the biasing voltage is 0.41 V, the measured IIP3 is found to be 39.5 dBm, which is comparable to that of a balanced BSF [24] and better than that of a traditional varactor-tuned filter [25]. The IIP3 values are limited by varactor nonlinearities and can be improved by using back-to-back varactors [26].

Table 1 shows a performance comparison between the proposed tunable BSF and those reported in the literature targeting constant ABW. As shown, the proposed BSF offers the widest stopband tuning range.

## 4. CONCLUSION

This paper presents a simple but effective method for designing frequency-tuning BSFs. Theoretical analysis and experimental results demonstrate that constant ABW is maintained as the stopband frequency is tuned. The proposed design requires no extra circuits to control coupling strength and allows easy cascading of doublets for high-order filters. A prototype using two doublets was tested, showing a constant ABW over a tuning range of 3.3–5.1 GHz with a 42.9% fractional tuning range. The proposed BSF is attractive for practical applications requiring adaptive interference suppression, such as 5G or radar systems.

## REFERENCES


[1] Jun, S. and K. Chang, "Reconfigurable bandstop filter with tunable center frequency and bandwidth using piezoelectric transducer," *Microwave and Optical Technology Letters*, Vol. 55, No. 11, 2670–2672, 2013.

[2] Wong, S. W. and L. Zhu, "Implementation of compact UWB bandpass filter with a notch-band," *IEEE Microwave and Wireless Components Letters*, Vol. 18, No. 1, 10–12, 2008.

[3] Zhang, T., J. Pan, B. Liu, H. Zhang, and Z. Zhu, "Miniaturized wideband pole-zero following tunable bandstop filter for 5G millimeter-wave application," *IEEE Transactions on Circuits and Systems II: Express Briefs*, Vol. 71, No. 8, 3725–3729, 2024.

[4] Doumanis, E., G. Goussetis, J. Vuorio, K. Hautio, O. Amper, E. Kuusmik, and J. Pallonen, "Tunable filters for agile 5G new radio base transceiver stations [Application Notes]," *IEEE Microwave Magazine*, Vol. 22, No. 11, 26–37, 2021.

[5] Al-Yasir, Y. I. A., N. O. Parchin, Y. Tu, A. M. Abdulkhaleq, I. T. E. Elfergani, J. Rodriguez, and R. A. Abd-Alhameed, "A varactor-based very compact tunable filter with wide tuning range for 4G and Sub-6 GHz 5G communications," *Sensors*, Vol. 20, No. 16, 4538, 2020.

[6] Abunjaileh, A. I. and I. C. Hunter, "Tunable bandpass and bandstop filters based on dual-band combline structures," *IEEE Transactions on Microwave Theory and Techniques*, Vol. 58, No. 12, 3710–3719, 2010.

[7] Lakshmi, C. R., D. Kavitha, D. Kannadassan, and T. G. Shivapanchakshari, "Tunable microwave bandstop filter for sub-6 GHz 5G applications," in *International Conference on Intelligent Computing and Advances in Communication*, 583–595, 2024.

[8] Archer, J. L., W. L. Bongianni, and J. H. Collins, "Magnetically tunable microwave bandstop filters using epitaxial YIG film resonators," *Journal of Applied Physics*, Vol. 41, No. 3, 1359–1360, 1970.

[9] Qiu, G., C. S. Tsai, B. S. T. Wang, and Y. Zhu, "A YIG/GGG/GaAs-based magnetically tunable wideband microwave band-pass filter using cascaded band-stop filters," *IEEE Transactions on Magnetics*, Vol. 44, No. 11, 3123–3126, 2008.

[10] Wei, F., C. Y. Zhang, C. Zeng, and X. W. Shi, "A reconfigurable balanced dual-band bandpass filter with constant absolute bandwidth and high selectivity," *IEEE Transactions on Microwave Theory and Techniques*, Vol. 69, No. 9, 4029–4040, 2021.

[11] Zeng, Z. and L. Bai, "Frequency-reconfigurable wideband bandstop filter using varactor-based dual-slotted defected ground structure," *IEICE Electronics Express*, Vol. 18, No. 10, 20210154, 2021.

[12] Shalaby, M., M. Abdelmoneum, and K. Saitou, "Design of spring coupling for high Q, high frequency MEMS filters," in *ASME International Mechanical Engineering Congress and Exposition*, Vol. 47756, 129–137, 2006.

[13] Choi, J.-Y., J. Ruan, F. Coccetti, and S. Lucyszyn, "Three-dimensional RF MEMS switch for power applications," *IEEE Transactions on Industrial Electronics*, Vol. 56, No. 4, 1031–1039, 2009.

[14] Reines, I., S.-J. Park, and G. M. Rebeiz, "Compact low-loss tunable X-band bandstop filter with miniature RF-MEMS switches," *IEEE Transactions on Microwave Theory and Techniques*, Vol. 58, No. 7, 1887–1895, 2010.

[15] Vali, S. S., G. Shanthi, A. Yalavarthi, S. Pingalakani, D. Chandrika, C. Ganesh, and K. G. Sravani, "Design and simulation of tunable bandstop filters by integrating RF MEMS shunt switch for K-band applications," *Microsystem Technologies*, Vol. 31, No. 4, 977–986, 2025.

[16] Annam, K., B. Alemayehu, E. Shin, and G. Subramanyam, "Tunable filters using defected ground structures at millimeter-wave frequencies," *Micromachines*, Vol. 16, No. 1, 60, 2024.

[17] Guermal, M., J. Zbitou, M. Hefnawi, and F. Aytouna, "A novel configuration of reconfigurable bandpass filter based on varactor diodes," *E-Prime — Advances in Electrical Engineering, Electronics and Energy*, Vol. 11, 100889, 2025.

[18] Zhang, X. Y., C. H. Chan, Q. Xue, and B.-J. Hu, "RF tunable bandstop filters with constant bandwidth based on a doublet configuration," *IEEE Transactions on Industrial Electronics*, Vol. 59, No. 2, 1257–1265, 2012.

[19] Brown, J. A., S. Barth, B. P. Smyth, and A. K. Iyer, "Compact mechanically tunable microstrip bandstop filter with constant absolute bandwidth using an embedded metamaterial-based EBG," *IEEE Transactions on Microwave Theory and Techniques*, Vol. 68, No. 10, 4369–4380, 2020.

[20] Zysman, G. I. and A. K. Johnson, "Coupled transmission line networks in an inhomogeneous dielectric medium," *IEEE Transactions on Microwave Theory and Techniques*, Vol. 17, No. 10, 753–759, 1969.

[21] Huang, F., "Dual-band superconducting spiral filters including narrow bandstop notches," *IEEE Transactions on Microwave Theory and Techniques*, Vol. 57, No. 5, 1188–1195, 2009.

[22] Pozar, D. M., *Microwave Engineering: Theory and Techniques*, John Wiley & Sons, 2021.

[23] Hickle, M. D. and D. Peroulis, "Tunable constant-bandwidth substrate-integrated bandstop filters," *IEEE Transactions on Microwave Theory and Techniques*, Vol. 66, No. 1, 157–169, 2018.

[24] Zhou, W.-J. and J.-X. Chen, "High-selectivity tunable balanced bandpass filter with constant absolute bandwidth," *IEEE Transactions on Circuits and Systems II: Express Briefs*, Vol. 64, No. 8, 917–921, 2017.

[25] Cho, Y.-H. and G. M. Rebeiz, "Two-and four-pole tunable 0.7-1.1-GHz bandpass-to-bandstop filters with bandwidth control," *IEEE Transactions on Microwave Theory and Techniques*, Vol. 62, No. 3, 457–463, 2014.

[26] El-Tanani, M. A. and G. M. Rebeiz, "A two-pole two-zero tunable filter with improved linearity," *IEEE Transactions on Microwave Theory and Techniques*, Vol. 57, No. 4, 830–839, 2009.